



OPEN

SUBJECT AREAS:
BIOLOGICAL SCIENCES
BIOLOGICAL TECHNIQUES
IMAGING
OPTICAL IMAGINGReceived
8 March 2013Accepted
19 July 2013Published
6 August 2013Correspondence and
requests for materials
should be addressed to
J.M. (joanne.
marrison@york.ac.uk)

Ptychography – a label free, high-contrast imaging technique for live cells using quantitative phase information

Joanne Marrison, Lotta Rätty, Poppy Marriott & Peter O'Toole

Imaging and Cytometry Laboratory, Bioscience Technology Facility, Department of Biology, University of York, UK.

Cell imaging often relies on synthetic or genetic fluorescent labels, to provide contrast which can be far from ideal for imaging cells in their *in vivo* state. We report on the biological application of a, label-free, high contrast microscopy technique known as ptychography, in which the image producing step is transferred from the microscope lens to a high-speed phase retrieval algorithm. We demonstrate that this technology is appropriate for label-free imaging of adherent cells and is particularly suitable for reporting cellular changes such as mitosis, apoptosis and cell differentiation. The high contrast, artefact-free, focus-free information rich images allow dividing cells to be distinguished from non-dividing cells by a greater than two-fold increase in cell contrast, and we demonstrate this technique is suitable for downstream automated cell segmentation and analysis.

Label-free imaging techniques are set to become more and more valuable in biological research as *in vitro* stem cell studies, drug discovery programs and studies where there is a requirement for minimal cell manipulation become increasingly important. There have been some significant advances recently in non-invasive, label-free imaging¹. Examples of these include digital holographic microscopy^{2–7} and ptychography^{8–10}.

For many cell imaging studies, for example cell state and cell cycle studies, image contrast is simply too low unless dyes are added. Routine dyes, such as the cell permeable DNA dyes DRAQ5 and Hoechst, are used extensively in fluorescence microscopy for crude analysis of live cells. Visualisation of the morphological changes that occur during apoptosis, cell death and cell division also typically rely on the use of fluorochromes to enhance contrast. For example, apoptotic cells can be labelled with Annexin V-FITC antibody staining^{11,12}, whilst viable and non-viable cells can be distinguished on the basis of membrane integrity using propidium iodide which can also be used for cell cycle analysis^{13,14}. Genetic engineering can be used to introduce fluorescent protein tags. For example, H2B-GFP has been used to analyse cell cycle behaviour and categorise nuclei into different phases using online detection algorithms¹⁵. Classification of cell cycle phases can also be achieved with the fluorescent ubiquitination cell cycle indicator (FUCCI) in which Cdt1-RFP marks G1 phase nuclei red and geminin-GFP marks S, G2 and M phase nuclei green¹⁶. Nuclei in G1/S appear orange when Cdt1-RFP and geminin-GFP are co-expressed. FUCCI has no apparent cell toxic effects but like H2B-GFP relies on transfection of cells which may not always be appropriate when screening new pharmaceuticals or assessing stem cell proliferation.

While such staining and labelling techniques produce high contrast images suitable for downstream analysis, they require the manipulation and interruption of 'normal' cell culture conditions potentially perturbing normal cell function and possibly disrupting the cell division process. There is therefore a requirement for non-invasive, label-free and artefact-free tools that can continuously monitor cell states *in vitro* that can yield contrast to rival fluorescent imaging, and that lend themselves to ease of use, automation and downstream quantitative analysis. Such label-free imaging techniques would be particularly appropriate for biological studies of, e.g., primary cells and *in vitro* stem cells, drug discovery programs, and studies where there is a requirement for minimal cell manipulation.

Many label-free approaches rely on the visualisation of contrast that is the result of phase changes introduced between the essentially transparent cells and their surrounding media. The most widely used classical label-free methods include differential interference contrast (DIC) and Zernike phase contrast. DIC is a beam-shearing interference technique which relies on optical path length gradients to enhance image contrast, and is especially useful for detecting cells edges and internal cell topography; Zernike phase contrast yields high-contrast images of cells based on optical path length magnitude so the dense cell areas with longer path lengths appear darker than the background. Such methods have been employed in automatic tracking of migrating cells¹⁷ and in mitosis



detection in stem cells¹⁸. However, the enhancement offered by DIC results in pseudo-3D images, while Zernike contrast suffers from halo artefacts at cell edges and neither methods are quantitative. Methods such as reflection interference contrast microscopy (RICM)¹⁹ and phase-shifted laser feedback interferometry (psLFIM)²⁰ although quantitative are limited to studying changes in the specimen at the coverslip-buffer interface such as cell adhesion and stress fibres. These techniques are not able to image through the depth of the cell and therefore cannot give a quantitative measure of cell volume changes that occur, for example, during cell division. These ubiquitous artefacts and limitations can compromise the success rate of downstream image analysis packages and are limited in their applications.

The recent emergence of new label-free imaging techniques can overcome some of these limitations. Examples of these include digital holographic microscopy (DHM)²⁻⁷ and the transport-of-intensity equation (TIE)²¹. For example, DHM has been used to provide quantitative phase images of live cells² *in vitro*, to detect cell division in endothelial cells³, to determine the refractive index using incorporated microspheres⁵ and to detect early cell death based on cell volume changes⁶. In DHM a reference beam is interfered with a beam scattered by a specimen such that the intensity of the resulting fringe pattern encodes information about the sample's phase-altering properties. The reliance on the interference of a reference wave in DHM means it typically requires a specifically designed machine aligned to high tolerances. In TIE-based techniques (which can be incorporated into existing microscopes) three images are recorded at and either side of focus effectively replacing the requirement for an interfering reference wave. The TIE has also been combined with DIC (TI-DIC) to obtain quantitative DIC images²². Although simple to implement, the accuracy of the TIE method diminishes as the Numerical Aperture (NA) of the microscope increases and the method is susceptible to noise.

In this paper, we describe a unique microscopy approach that uses an iterative phase retrieval method known as ptychography⁸⁻¹⁰ that is also being used for microscopy at X-ray²³ and electron wavelengths²⁴. The specimen and a coherent illuminating beam (probe) are moved with respect to one another to create on the specimen a sequential array of overlapping illuminated areas. For each illuminated area, the light scattered as it passes through the specimen is captured as a diffraction pattern on a CCD camera. The diffraction patterns are then processed using a ptychographic algorithm – in the present case, the extended ptychographic iterative engine (ePIE)^{9,10}.

A key property of ptychography is that it recovers the phase of the wave that has travelled through the specimen with great accuracy and with high contrast. This means that it can be used for the structural discovery of very weakly absorbing specimens – in the present study, essentially transparent cells. Another key property is that image resolution is determined only by the effective numerical aperture of the detector.

The task of image formation is performed by the ptychographic computer algorithm, eliminating the requirement for the customary objective lens. However, when a ptychography capability is integrated with a conventional microscope as in the present case (Fig. 1), an existing objective lens mounted on the standard microscope turret may be usefully employed to collect the exit wave leaving the specimen, where an image of the specimen is subsequently formed at the back focal plane of the tube lens. Using this geometry, localised areas of the image can be selected by a diaphragm and scanned across the specimen by translation of the specimen stage¹⁰.

The output of the ePIE algorithm is a pair of images; one is a quantitative measure of the extent to which light has been absorbed by the specimen (an equivalent of a conventional brightfield image) and other is a quantitative measure of the phase delay introduced into the illumination as it passes through the specimen. The image pair can be refocused post-acquisition at any user-selected depth; this

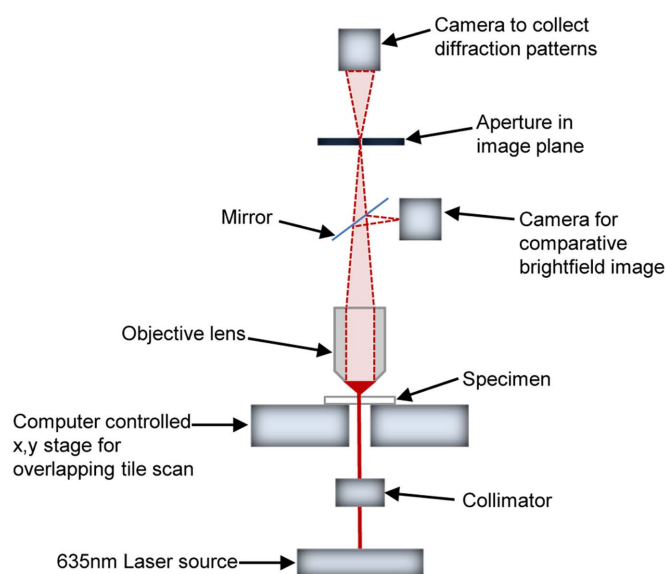


Figure 1 | Basic configuration of the ptychographic microscope. A schematic diagram of the light path in the ptychographic microscope showing the laser, collimator, x,y scanning stage, objective lens, the aperture in the image plane and the 2 CCD cameras.

capability can be used to analyse three-dimensional characteristics of the specimen, and has potential to aid cell imaging through the depth of a culture flask. In addition to outputting images of the specimen, ePIE also calculates the complex waveform of the illumination used, thereby providing high quality reconstructions when the form of the illumination is not known, and compensating automatically for a number of imperfections in the optical system.

Unlike DHM, ptychography reconstructs the phase and amplitude of a scattered wavefield without the need of a reference wave and is therefore inherently more stable, less prone to artefacts and optically less complex thus enabling easy modification of standard microscopes and can be used in conjunction with fluorescence microscopy. Moreover, the recovered phase in ptychography typically exhibits significantly lower noise than that obtained via digital holography due to the elimination of speckle. Ptychography is not susceptible to the loss of accuracy at high NA suffered by TIE, and is very immune to noise. Indeed, up to 50% of random noise added to each detector pixel reading can produce interpretable images²⁵.

Ptychographic phase images are of very high contrast, and free of the artefacts. The quantitative nature of ptychographic data reflects thickness and refractive index variations in the specimen; such changes that are associated with cell division provide contrast in the label-free imaging reported here. We show this technique lends itself readily to subsequent segmentation and image analysis and thus provides the basis for non-destructive automated monitoring of cell states in culture an important feature in proliferation and migration assays, the study of primary cells, disease states, the study of response to various drugs/effector molecules and in tracking mixed cell populations.

Results

Comparison of ptychography with traditional contrast enhancement techniques. Ptychographic images of A549 cells were compared with brightfield, phase contrast and DIC images (Fig. 2). As expected in the brightfield image the cells appeared semi-transparent, with only the transitional regions between areas of significantly different refractive index (such as the membrane and nucleus) being visible (Fig. 2a). The brightfield image was slightly defocused to give the cell edges increased contrast. The same field of view showed more contrast and structural detail when observed with



phase contrast and DIC optics (Fig. 2b,c). The phase contrast image showed the characteristic bright halo around the edge of the cells (Fig. 2b arrows). When viewed using DIC the cells had pseudo 3-D relief but a similar tonal range to the background (Fig. 2c). The ptychographic image (Fig. 2d) which reports grey level as a function of phase shift, had a uniformly dark background and the cells were in bright relief, similar to a fluorescent image. Crucially the ptychographic image had none of the halo artefacts and shadow casts associated with the conventional contrast enhancement techniques. The ptychographic image showed 5 cells with higher contrast than the others (Fig. 2d, arrows), which may be cells rounding up and entering G2/M. This distinction in cell state was not readily seen in the phase contrast image (Fig. 2b). The pseudo 3-D effect of the DIC image did enhance the nucleus of these cells (Fig. 2c, arrows) but because the contrast was low the difference was not readily perceived

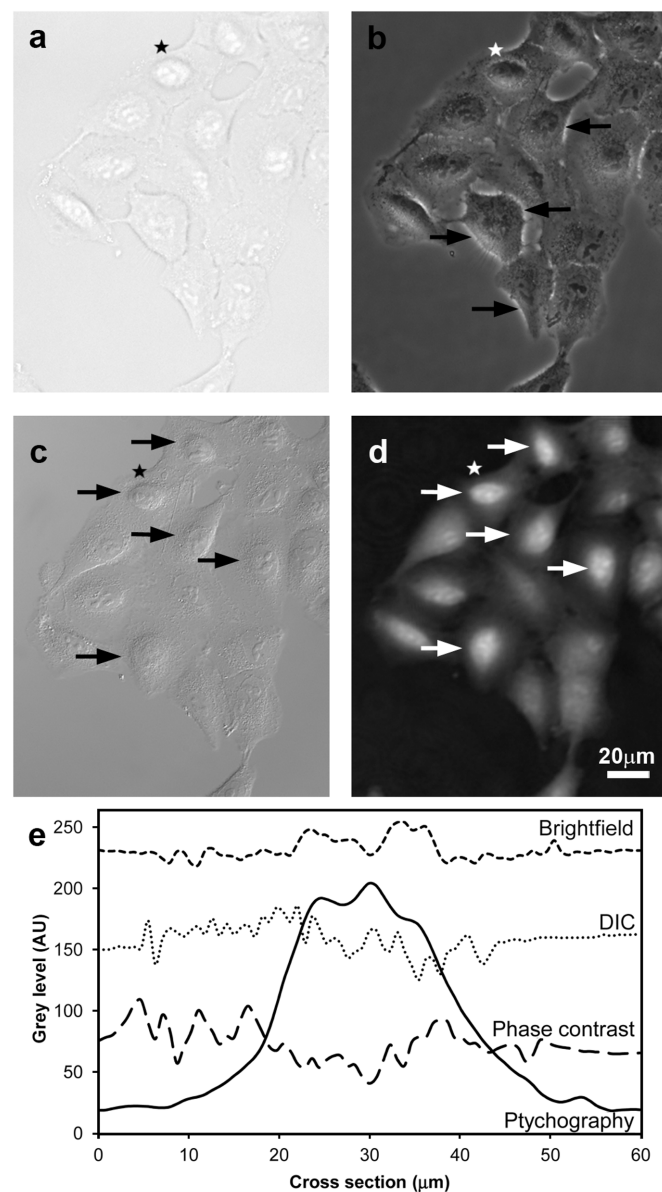


Figure 2 | Comparison of traditional contrast enhancement techniques with ptychography. (a) Brightfield image defocused to reveal cell edges. (b) Zernike phase contrast image (arrows point to characteristic halo artefact around the cell edges). (c) DIC image. (d) Ptychographic image. All images (a–d) are recorded from the same field of view. (e) The variation in grey level across a cell (marked by an asterisk a–d) and adjacent background for all 4 imaging modalities.

until retrospectively compared to the ptychographic image. Grey level profiles (Fig. 2e) taken from across a cell and neighbouring background region (Fig. 2a–d star) showed the enhanced contrast obtained with ptychography compared to brightfield, phase contrast and DIC imaging. Critically, in the ptychographic image profile, all pixels within the cell appeared brighter compared to off-cell regions. There was a 10× increase in grey level in the ptychographic image from the background to the brightest point in the cell, the nucleolus. All other imaging modalities showed a variable grey level which was not correlated with background or on-cell regions.

Identification of different cell states using ptychography. To study the efficacy of ptychographic imaging in more detail, unstained cells were imaged in different states. At 37°C a typical image taken from a slide mounted specimen with a Plan CN 10×/0.25 objective and 18 × 18 probe point grid showed most of the live cells had a similar grey level but a small proportion appeared brighter than the rest of the population. These cells were in various stages of mitosis and were immediately identified from the rest of the cells (Fig. 3a, white arrows). Visualising the stages of mitosis has proved to be one of the major advantages and potential benefits of ptychography over classic label-free imaging techniques. A gradual increase in whole cell grey level was seen as the cells entered division. Spindle formation was highlighted by bright circular outlines within the nucleus (data not shown). Cells in metaphase were recognised by an intense line at the centre of the cell indicative of chromosome condensation and alignment at the metaphase plate (Fig. 3a, yellow arrowhead). Chromosome separation in anaphase and telophase was identified by two lines of increased grey level within the dividing cells as the chromatids moved towards the poles (Fig. 3a red arrowheads). The cells also began to elongate and pinch in (Fig. 3a white arrows) to generate the two daughter cells. The mitotic process was observed all the way through to cytokinesis when the grey levels of the daughter cells decreased as they returned to G1 (Fig. 3a green arrows). As an exaggerated “cell culture” model, cells were imaged in an 8-well chambered coverslip through approximately 1 cm of culture media, where mitotic cells appeared brighter and chromosome alignment was also observed in these imaging conditions (Fig. 3a inset, arrowheads). Cells imaged at 42°C showed characteristic vesiculation of the cytoplasm due to heat shock (Fig. 3b arrows) and rounder, brighter apoptotic cells showed distinctive blebbing of the cell membrane (Fig. 3c arrows). Ruffles on the leading edges of cells were seen when non-confluent cell preparations were imaged with ptychography (Fig. 3d arrows), the ruffles showed very poor contrast in DIC (Fig. 3e) and were not seen at all with Zernike phase contrast (data not shown) as they were obscured by the halo around the edge of the cells.

Quantitative assessment of cell division using ptychography. The ease with which cells in different stages of mitosis were reliably identified along with the high contrast and lack of artefacts suggested ptychographic imaging would be an ideal starting point for label-free image segmentation and analysis of the cell cycle.

The ptychographic images were analysed using Columbus software (PerkinElmer). The software successfully segmented cells out to the edges of the images, reliably separating neighbouring cells. Cells touching the image border were removed to ensure only whole cells were analysed (Fig. 4a).

The A549 cells have a doubling time of approximately 18 hours²⁶ so, in order to track cell division, cells were maintained at 37°C and ptychographic images were taken automatically every 5 minutes for a period of 20 hours (see Supplementary video S1 online). This permitted most cells to undergo at least one round of division as the cells were not synchronised for cycle time. At the beginning of the time course there were 56 cells in the imaged field and after 10 h the 121st image contained 101 cells demonstrating that the majority of cells in the field of view had entered and completed one round of division.

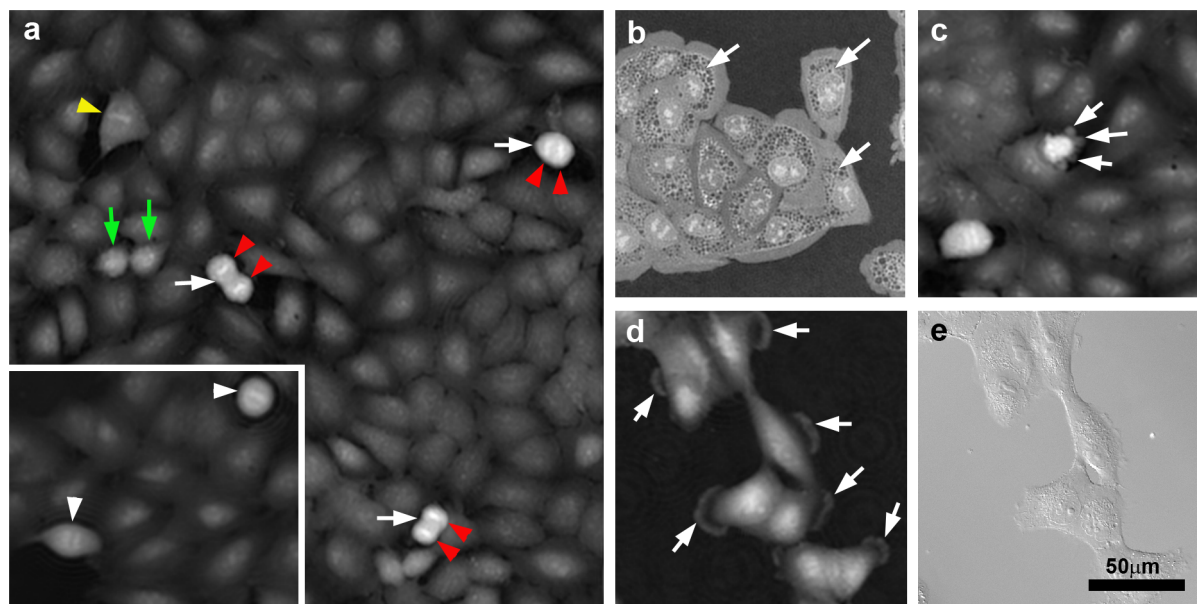


Figure 3 | Identification of cell states using ptychography. (a) A549 cells imaged at 37°C showing a proportion of brighter dividing cells (white arrows) and intense lines within the cells marking chromosome alignment prior to cytokinesis (arrowheads). Inset in (a) shows cells imaged through approximately 1 cm of media in an 8-well chambered coverslip. (b) Cells imaged at 40°C showing vesiculation of the cytoplasm due to heat shock (arrows). (c) Apoptotic cell which appears rounder and brighter than the surrounding healthy cells and shows membrane blebbing (arrows). (d) Cells in a non-confluent preparation showing membrane ruffles (arrows). (e) DIC image of the same field of view as (d) where membrane ruffles are barely visible.

The first 121 images (10 h) were analysed. The grey level and cell area were obtained for 12 representative non-dividing cells and 6 dividing cells which entered and exited division within the time frame along with the resulting 12 daughter cells. The data from dividing cells were aligned at the point where the daughter cells were recognised by the software as two cells, cytokinesis. The grey level/cell area increased 2.5-fold in dividing cells during the 30 minute time period between entry into cell division and cytokinesis compared to normalised background grey levels (Fig. 4b). Upon separation into two daughter cells the grey level/cell area decreased and continued to decline until the cells exited mitosis after 90 minutes. The grey level/cell area of the non-dividing cells remained low throughout the observation period (Fig. 4b).

A further 17 ‘snap-shot’ images from multiple slide preparations were segmented and analysed to show the variability in grey level/cell area over a range of cell sizes for both dividing and non-dividing cells. Cells were manually classified into dividing or non-dividing cells; bright, rounded cells and cells containing the lines indicative of chromosome condensation and alignment at the metaphase plate and cells which were part of a pair of rounded daughter cells were all classified as dividing cells, while the remainder were classified as non-dividing cells. On this basis 58 dividing cells and 505 resting cells were analysed (Fig. 4c). The mean grey level (arbitrary units/cell area, $\text{AU}/\mu\text{m}^2$) of non-dividing cells was $95.0 \text{ AU}/\mu\text{m}^2$ (SE 4.86), whereas the mean grey level of dividing cells was twice this at $196.9 \text{ AU}/\mu\text{m}^2$ (SE 4.86). The average cell area of dividing cells was $398.9 \mu\text{m}^2$ (SE 19.65) and the average cell area of non-dividing cells $840.2 \mu\text{m}^2$ (SE 9.47). Boundaries were drawn around each of the two populations. 12.1% (7/58) of dividing cells fell within the boundaries of the non-dividing cell population and 6.9% (35/505) of non-dividing cells fell within the boundaries of the dividing cell population. These data were taken from ‘snapshot’ images for which cell history was not established so with further time lapse imaging many of these cells may have been categorised as entering early mitosis.

We plotted the changes in mean grey level and cell area for 3 of the dividing cells over time (Fig. 4d–f). Prior to and after cell division the cell maintained a relatively consistent mean grey level and any

changes in cell area were probably due to cell motility. As the cell entered division the mean grey level increased rapidly followed by a decrease in cell area as the cells round up at cytokinesis. After division the mean grey level dropped and the cell area increased again.

Discussion

The use of ptychography can significantly improve how we visualise, analyse and study cells. Unstained cells absorb very little light and are essentially transparent in conventional brightfield microscopy. Although enhancing techniques such as DIC and phase contrast can increase contrast they are unsuitable for many applications. Phase contrast results in a halo effect around the cells which can obscure cellular detail, whilst DIC gives little contrast compared to background intensities making segmentation of individual cells difficult and unreliable. Fluorescence microscopy is frequently used to enable segmentation of closely spaced cells, however, this requires cells to be labelled with fluorescent dyes which is far from ideal and can be expensive when running large screens. Many therapeutic assays depend on using endogenous labels that have the potential to perturb the natural state and function of the cell of interest and are not always possible or desired in specific assays. We have shown that using ptychography not only results in high contrast images of unlabelled cells but can yield further biological information without the need for staining. The images are similar to those of fluorescently labelled cells with cells showing an increase in grey level throughout the on-cell region compared to a relatively dark black background. Ptychography also enables us to use low cost, low magnification lenses with large working distances, ideal for many screening studies.

A549 cells were used in this study for their adherent and robust nature making time-lapse studies relatively simple. We chose to use a 635 nm red laser line for imaging to minimise any potential cell damage compared to shorter wavelength, higher energy laser lines. The ability to track cells through several rounds of replication gave us confidence that the imaging has no detrimental effect on the cells. A laser power in the order of $15 \text{ pW}/\mu\text{m}^2$ was recorded (Fieldmate meter, OP-2VIS sensor, Coherent) exiting the collimating lens. Longer, lower energy wavelengths are naturally possible but deemed

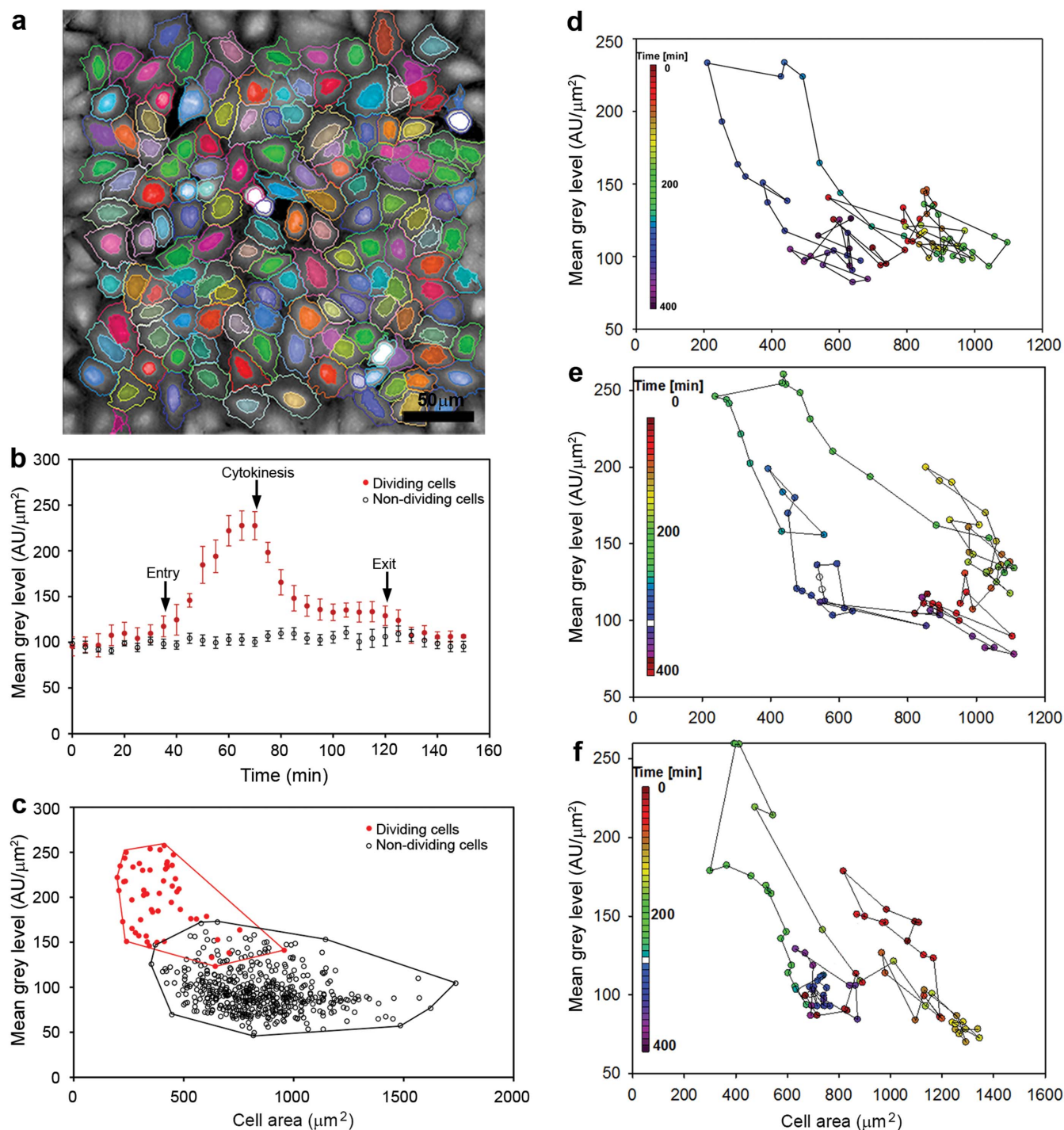


Figure 4 | Quantification of dividing and non-dividing cells using ptychography and segmentation. (a) Shows the image from Fig. 3a after segmentation with Columbus image analysis software. (b) Mean grey levels during cell division for 6 cells and their 12 daughter cells at 5 minute intervals. The time points of entry into cell division, cytokinesis and exit from cell division are marked. Mean grey levels are also shown for 12 non-dividing cells. (c) Cell area and mean grey level for a population of 58 dividing cells and a population of 505 non-dividing cells. (d–f) Trajectories showing how cell area and cell mean grey level change over time during cell division for 3 representative cells. Each time point in the image series is represented by a coloured data point according to the scale at the left hand side of the graphs in d–f. White data points indicate unavailable time points.

unnecessary. A shorter wavelength laser could potentially improve resolution, but would also increase the potential for cellular damage; this has not been investigated.

To produce each ptychographic image a series of diffraction patterns were collected and the size of the area covered was usually sufficient to image a group of clustered cells. The speed of acquisition was around 100 seconds for the image shown in fig. 3a; this is fit for

purpose but later modifications have been made by the supplier (Phase Focus Ltd, Sheffield, UK, www.phasefocus.com) and 30 second capture is now possible. Therefore with the use of a 10× long working distance lens large areas of interest can now be captured significantly faster and future modifications are expected to decrease this time even further. The raw data is merely a scattered light pattern which must be processed in order to reconstruct the image before any



cellular analysis can be undertaken. The reconstructed data can be manipulated to virtually focus the cells post-acquisition with respect to their z-plane. This is an important aspect of the system; cells only require crude focussing whilst the algorithms will then allow fine focussing over a large range (100 μm). This in itself is invaluable as each image area does not need to be refocused nor would an automated autofocus procedure be needed for large screening or time-lapse protocols. We manipulated the virtual focus manually to find the best focal plane for each image after reconstruction, but this can now also be done via an automated virtual auto-focus algorithm after imaging. If the field of view is uneven, no data will be lost through focussing issues as the algorithm can also be used to bring other areas of interest into focus with no need to change the Z-position and re-image. Therefore with all cells now available to analyse, along with autofocus, critical time savings can now be made to increase throughput and offset current speed limitations.

It was noticeable that the ptychographic background does not have any normalisation within the current algorithms, and so for further analysis background subtraction was used to normalise the grey levels with multiple data sets. The results gave good high contrast images of the adhered cells. Cells were noted to increase in grey level as they become thicker. This was presumed to be as a result of the induced phase change as the light passes through a thicker region of the sample with a varied refractive index. The image becomes significantly brighter at the cell nucleus which is most likely due to increased thickness and/or a higher refractive index due at least in part to the increased curvature of the surrounding membrane. The relatively bright nucleus easily enables cells to be identified and the decreasing grey level towards the edge readily permits segmentation for further cell analysis.

An added advantage of using ptychography is that cells can be imaged through various materials such as cell culture plastic ware. The reconstructed images show changes in phase, so a uniform thickness of plastic results in negligible change in contrast which results in an even background from which images of cells can be easily formed. This is a significant advantage over other methods when cells do not adhere well on glass surfaces.

Cells entering division naturally start to increase in volume, whilst also rounding up. This increased thickness of the cell and increased curvature results in a larger phase change which in turn results in a brighter area with increased contrast. Therefore, cells entering division can be identified visually by their relatively increased brightness compared to cells not undergoing division. Tracking cell division over time demonstrated that the mean grey level of dividing cells increased 2.39 fold ± 0.31 at the point of cytokinesis before returning to the resting cell mean grey level after division. The natural ability to see such grey level changes is comparable to classic cytometric DNA cell cycle studies using fluorescent DNA stains. Indeed it is encouraging that the grey level increase is greater than that seen when using DNA stains which naturally show a doubling of intensity reflecting the doubling of DNA through G2/M. The ability to differentiate between cells in different stages of cell cycle is an exciting prospect.

A scatter plot of mean grey level against cell area for cells from multiple slide preparations showed the profiles of dividing and non-dividing cells were clearly different with only minimal overlap. This was highlighted with two regions of interest (ROI) on the scatter plot, one encompassing all data from dividing cells and one encompassing all data from non-dividing cells (both manually classified). Cells classified as dividing but exhibiting grey levels in the lower sector of the ROI are most likely only just starting to enter mitosis or are returning to G1. This leads to a blurring of the mean grey levels between dividing and non-dividing cells and will in part account for the overlap of dividing/non-dividing cells. However, if only the latter stages of cell division immediately prior to cytokinesis are classified, or data is taken from a time course the results are absolute.

When mean grey level and cell area were tracked for individual cells it was seen that the cell mean grey level increases as the cell area decreases upon division. After division the increase in mean grey level stays similar but the daughter cells are naturally reduced in size. This trend enables us to further sub-divide the scatter plot mentioned above and to identify the cells entering mitosis and the returning daughter cells. Those cells lying in the right hand side of the dividing cell ROI are more likely to be entering mitosis and cells lying towards the left hand side of the dividing cell ROI are more likely to be the smaller daughter cells.

Not only do cells increase in grey level upon cell division, but the mitotic spindle also forms a striking feature. The increased contrast created by the mitotic spindle is possibly due to the regularity and density of the structure increasing its refractive index and consequently the induced phase shift as light passes through. The ability to readily pick out the mitotic spindle adds to the appeal for using phase algorithms for cell cycle studies. From imaging cells at various points through cell cycle, we can see the various spindle patterns associated with the sequential stages of mitosis. Again, the ability to study this without the need of fluorescent labels is very appealing. This ability to readily track cells through cell cycle will enable cycling times to be closely monitored for drug trials.

Ptychography has tremendous potential. The system generates high quality images using inexpensive, low magnification objective lenses without the need for the addition of cytotoxic labels, a technical advance which has far reaching implications for cancer research and drug discovery. Not only are the images high in contrast, but they are also artefact free making them ideal for downstream segmentation and image analysis. The ability to focus post-acquisition allows all cells, even in an uneven field, to be brought into focus and not omitted from subsequent analysis. Time is also saved pre-acquisition as cells can be imaged directly in tissue culture plastic ware. We have shown here that this technique is suitable for cell cycle analysis, identifying cells entering and exiting mitosis and dissecting the phases of mitosis. Ptychography would be ideal for in-incubator assays, reporting over prolonged periods of time on cell proliferation and cell cycle stages *in situ*. These are only initial studies but clearly demonstrate the potential of label-free ptychographic imaging. With the technology rapidly developing, faster acquisition times, smart auto-focus, increased contrast and ease of use, and the ability to add the facility to other systems e.g. confocals, make the future opportunities diverse and very attractive.

Methods

Cell culture and sample preparation. Adherent human alveolar epithelial cells (A549, a gift from D. Zicha, LRI) were cultured in Dulbecco's modified Eagle medium (D-MEM, Gibco) supplemented with foetal calf serum (10% (v/v), Gibco) and uridine (0.2 mM, Sigma). Cells were maintained at 37°C, 5% CO₂ and 90% humidity and passaged every 3–5 days after release with Trypsin-EDTA (Gibco) for 2 minutes at 37°C.

Cells for microscopy were cultured for 24 h, 48 h or 72 h on sterile coverslips (22 \times 22 mm, number 1.5, SLS) in 6-well cell culture dishes (Corning Costar). The coverslips were removed from the dishes and inverted with the cells facing towards a clean glass slide and mounted in culture medium and sealed with a ring of silicon high vacuum grease (Dow Corning). The outer surface of the coverslip was wiped clean. Cells were also cultured for 48 h in 8 well Lab-Tek II chambered coverslips (Nalge Nunc Int.). Before imaging the chamber lid was removed and the wells completely filled with media and sealed using a coverslip (22 \times 50 mm, number 1.5, SLS) to eliminate the meniscus.

Microscopy. For ptychographical imaging a conventional Olympus BX41 fluorescence microscope was customised with a 635 nm, 2.5 mW diode laser (Thorlabs), collimating lens which replaced the microscope condenser, computer controlled x-y microscope stage (Physik Instrumente) to allow movement of the specimen in relation to the laser, iris diaphragm and 2 monochrome, 16-bit, 1 megapixel Pike AVT (F-100B) CCD cameras: one to capture the diffraction pattern and the second for image capture¹⁷ (Phase Focus Ltd, Sheffield, UK, www.phasefocus.com) as shown in Figure 1. The slide was placed in an adapted stage top incubator (Zeiss Tempcontrol 37-2 Digital and CTI Controller 3700 Digital) held at 37°C or 42°C at the specimen for short-term live cell imaging. An overlapping 18 \times 18 tiled scan was collected by stepping the stage in x,y to generate the images



presented here. The spacing between each position was objective lens dependent, typically 70–150 μm , and was calculated from a region of interest (ROI) selected on a live video feed image. The dwell time at each probe point was 0.05 s. The exit wave leaving the specimen was collected with either an Olympus Plan CN 10 \times /0.25 or Plan N 20 \times /0.4 objective, resulting in reconstructions with pixel spacing of 0.79 μm and 0.39 μm respectively. A total of 324 (18 \times 18) diffraction patterns were recorded for each reconstructed image; one from each overlapping probe position (resulting in an average acquisition time of 100 s primarily limited by X, Y stage movement speed). For time lapse imaging, diffraction patterns were recorded automatically every 5 minutes from the 18 \times 18 probe point ROI over 20 hours.

Image reconstruction was completed using 150 iterations of the extended Ptychographical Iterative Engine (ePIE)^{9,10} supplied by Phase Focus Ltd (marketed as The Phase Focus Virtual Lens[®], Phase Focus, Sheffield, UK, www.phasefocus.com). Images were saved in 8-bit TIF (Tagged Image File) format. Images can be saved in 8-bit or 16-bit as required.

Correlative brightfield and Zernike phase contrast images were taken using a Zeiss Axiovert 200 with a Zeiss Plan Apochromat 20 \times /0.6 PH2 objective; DIC images were taken using a Zeiss AxioPlan 2 with a Zeiss Plan Neofluar 40 \times /1.3 oil DIC objective. All images were captured using a Zeiss AxioCam HRm CCD camera and Axiovision software.

Image analysis. To compare the dynamic range of grey levels for different imaging techniques, brightfield (Plan Apochromat 20 \times /0.6 PH2 objective), phase contrast (Plan Apochromat 20 \times /0.6 PH2 objective), DIC (Plan Neofluar 40 \times /1.3 oil DIC objective) and ptychographic (Plan CN 10 \times /0.25) images of the same field of view were imported into Image J (V. 1.41, NIH). The pixel grey level profile was generated by drawing a 60 μm line across the same cell and background in the different imaging modalities. As the cameras used had different pixel resolutions all images were converted to 0.79 μm /pixel, the ptychographic pixel size, in SigmaPlot V11 (Systat software Inc.) for valid comparison of the various techniques.

Ptychographic images were imported into Columbus V2.3 software (PerkinElmer) for image analysis using 'find nuclei' and 'find cytoplasm' script blocks. Cells touching the edge of the image were excluded in a 'select population' script block using 'remove border objects' to ensure only whole cells were analysed. Cell area and cell grey level was recorded.

- Greenbaum, A. *et al.* Imaging without lenses: achievements and remaining challenges of wide-field on-chip microscopy. *Nat. Methods* **9**, 889–895 (2012).
- Marquet, P. *et al.* Digital holographic microscopy: a noninvasive contrast imaging technique allowing quantitative visualisation of living cells with subwavelength axial accuracy. *Opt. Letts.* **30**, 468–470 (2005).
- Kemper, B. *et al.* Label-free quantitative cell division monitoring of endothelial cells by digital holographic microscopy. *J. Biomed. Opt.* **15**, 036009 (2010).
- Alm, K. *et al.* *Digital Holography and Cell Studies, Holography, Research and Technologies*, J. Rosen (Ed.), pp237–252. InTech (2011).
- Przibilla, S. *et al.* Sensing dynamic cytoplasm refractive index changes of adherent cells with quantitative phase microscopy using incorporated microspheres as optical probes. *J. Biomed. Opt.* **17**, 097001 (2012).
- Pavillon, N. *et al.* Early cell death detection with digital holographic microscopy. *PlosOne* **7**, e30912 (2012).
- Cotte, Y. *et al.* Marker-free phase nanoscopy. *Nature Photonics* **7**, 113–117 (2013).
- Rodenburg, J. M., Hurst, A. C. & Cullis, A. G. Transmission microscopy without lenses for objects of unlimited size. *Ultramicroscopy* **107**, 227–231 (2007).
- Maiden, A. M. & Rodenburg, J. M. An improved ptychographical phase retrieval algorithm for diffractive imaging. *Ultramicroscopy* **109**, 1256–1262 (2009).
- Maiden, A. M., Rodenburg, J. M. & Humphry, M. J. A new method of high resolution, quantitative phase scanning microscopy. *Proc. SPIE* **7729**, Scanning Microscopy (2010).
- Koopman, G. *et al.* Annexin V for flow cytometric detection of phosphatidylserine expression on B cells undergoing apoptosis. *Blood* **84**, 1415–1420 (1994).
- Gatti, R. *et al.* Comparison of annexin V and calcein-AM as early vital markers of apoptosis in adherent cells by confocal laser microscopy. *J. Histochem. Cytochem.* **46**, 895–900 (1998).
- Shapiro, H. M. *Practical Flow Cytometry 4th edition*. J.Wiley & sons (2003).
- Krishnan, A. Rapid flow cytofluorometric analysis of mammalian cell cycle by propidium iodide staining. *J. Cell Biol.* **66**, 188–193 (1975).
- Wang, M. *et al.* Novel cell segmentation and online SVM for cell cycle phase identification in automated microscopy. *Bioinformatics* **24**, 94–101 (2008).
- Sakaue-Sawano, A. *et al.* Visualising spatiotemporal dynamics of multicellular cell-cycle progression. *Cell* **132**, 487–498 (2008).
- Hand, A. J., Sun, T., Barber, D. C., Hose, D. R. & Macneil, S. Automated tracking of migrating cells in phase-contrast video microscopy sequences using image registration. *J. Microsc.* **234**, 62–79 (2009).
- Huh, S., Ker, D. F. E., Bise, R., Chen, M. & Kanade, T. Automated mitosis detection of stem cell populations in phase-contrast microscopy images. *IEEE Trans. Med. Imag.* **30**, 586–596 (2011).
- Limozin, L. & Sengupta, K. Quantitative reflection interference contrast microscopy (RICM) in soft matter and cell adhesion. *ChemPhysChem* **10**, 2752–2768 (2009).
- Atilgan, E. & Ovryn, B. Reflectivity and topography of cells grown on glass-coverslips measured with phase-shifted laser feedback interference microscopy. *Biomed. Opt. Express* **2**, 2417–2437 (2011).
- Beleggia, M., Schofield, M., Volkov, V. & Zhu, Y. On the transport of intensity technique for phase retrieval. *Ultramicroscopy* **102**, 37–49 (2004).
- Kou, S., Waller, L., Barbastathis, G. & Sheppard, C. J. R. Transport-of-intensity approach to differential interference contrast (TI-DIC) microscopy for quantitative phase imaging. *Opt. Letts.* **35**, 447–449 (2010).
- Maiden, A. *et al.* Soft X-Ray spectromicroscopy using ptychography with randomly phased illumination. *Nat. Commun.* **4**, 1669 Doi:10.1038/ncomms2640 (2013).
- Humphry, M. J., Kraus, B., Hurst, A. C., Maiden, A. M. & Rodenburg, J. M. Ptychographic electron microscopy using high-angle dark-field scattering for sub-nanometre resolution imaging. *Nat. Commun.* **3**, 730 Doi:10.1038/ncomms1733 (2012).
- Faulkner, H. M. L. & Rodenburg, J. M. Error tolerance of an iterative phase retrieval algorithm for moveable illumination microscopy. *Ultramicroscopy* **103**, 153–164 (2005).
- Orfanoudakis, G., Zaoui, D., Befort, J.-J. & Bieth, J. G. Cell cycle-specific variation of intracellular plasminogen activator activity in cultured human alveolar epithelial carcinoma and rat hepatoma cells. *Biology of the cell* **65**, 279–300 (1989).

Acknowledgements

We thank Ian Pykett, Martin Humphry and James Russell (Phase Focus Ltd, Sheffield) for technical support. We also acknowledge Andrew King (University of York) for preliminary experimental work and the Imaging and Cytometry Laboratory especially Ian Morrison (Bioscience Technology Facility, University of York) for helpful discussions. The work was funded by METRC N8 funding to Peter O'Toole and Phase Focus.

Author contributions

J.M. and P.O.T. conceived and designed the experiments, J.M., L.R. and P.M. performed the experiments, J.M. analysed the data, J.M. and P.O.T. wrote the paper.

Additional information

Supplementary information accompanies this paper at <http://www.nature.com/scientificreports>

Competing financial interests: The authors declare no competing financial interests.

How to cite this article: Morrison, J., Rätty, L., Marriott, P. & O'Toole, P. Ptychography – a label free, high-contrast imaging technique for live cells using quantitative phase information. *Sci. Rep.* **3**, 2369; DOI:10.1038/srep02369 (2013).



This work is licensed under a Creative Commons Attribution-NonCommercial-ShareAlike 3.0 Unported license. To view a copy of this license, visit <http://creativecommons.org/licenses/by-nc-sa/3.0>